Aerosol Science and Technology

ISSN: 0278-6826 (Print) 1521-7388 (Online) Journal homepage: http://www.tandfonline.com/loi/uast20

Volatility characterization of nanoparticles from single and dual-fuel low temperature combustion in compression ignition engines

Glenn Lucachick, Scott Curran, John Storey, Vitaly Prikhodko & William F. Northrop

To cite this article: Glenn Lucachick, Scott Curran, John Storey, Vitaly Prikhodko & William F. Northrop (2016): Volatility characterization of nanoparticles from single and dual-fuel low temperature combustion in compression ignition engines, Aerosol Science and Technology, DOI: 10.1080/02786826.2016.1163320

To link to this article: http://dx.doi.org/10.1080/02786826.2016.1163320

Volatility characterization of nanoparticles from single and dual-fuel low temperature combustion in compression ignition engines

Glenn Lucachick[a], Scott Curran[b], John Storey[b], Vitaly Prikhodko[b], William F. Northrop[a]

[a]Department of Mechanical Engineering, University of Minnesota, Minneapolis, Minnesota, USA

[b]Oak Ridge National Laboratory, Fuels, Engines and Emissions Research Center, Knoxville, Tennessee, USA

CONTACT William F. Northrop wnorthro@umn.edu Department of Mechanical Engineering, University of Minnesota, 111 Church St. SE, Minneapolis, Minnesota, 55455 USA.

ABSTRACT

This work explores the volatility of particles produced from two diesel low temperature combustion (LTC) modes proposed for high-efficiency compression ignition engines. It also explores mechanisms of particulate formation and growth upon dilution in the near-tailpipe environment. The number distribution of exhaust particles from low- and mid-load dual-fuel reactivity controlled compression ignition (RCCI) and single-fuel premixed charge compression

ignition (PPCI) modes were experimentally studied over a gradient of dilution temperature. Particle volatility of select particle diameters was investigated using volatility tandem differential mobility analysis (V-TDMA). Evaporation rates for exhaust particles were compared with V-TDMA results for candidate pure n-alkanes to identify species with similar volatility characteristics. The results show that LTC particles are mostly comprised of material with volatility similar to engine oil alkanes. V-TDMA results were used as inputs to an aerosol condensation and evaporation model to support the finding that smaller particles in the distribution are comprised of lower volatility material than large particles under primary dilution conditions. Although our results show that saturation levels are high enough to drive condensation of alkanes onto existing particles under the dilution conditions investigated, they are not high enough to allow homogeneous nucleation of these same compounds in the primary exhaust plume. Therefore, we conclude that observed particles from LTC operation must grow from low concentrations of highly non-volatile compounds present in the exhaust.

ARTICLE HISTORY

Received 27 July 2015

Accepted 3 February 2016

EDITOR Matti Maricq

INTRODUCTION

Conventional diesel combustion (CDC) in compression ignition (CI) engines results in the formation of carbonaceous soot agglomerates from diffusion-controlled burning which then combine with semi-volatile organics upon primary dilution in the exhaust plume. The resulting aerosol exhibits the familiar bi-modal particle size distribution (Kittelson, 1998) and is well-known to have adverse human health effects. Low temperature combustion (LTC) modes are of interest for use in CI engines due to their excellent fuel efficiency, and reduced soot and NO_X emissions versus conventional combustion. Further studies are necessary to fully determine whether LTC modes can reduce total PM. These modes rely on a high degree of dilution and premixing of air and fuel resulting in a largely kinetically controlled combustion process that avoids high temperature and fuel rich regions of the cylinder known to form soot (Musculus et al., 2013). Other well-known advantages of LTC modes include lower NO_X emissions and high engine efficiency. A number of strategies have been proposed to enable LTC in CI engines. Partially premixed compression ignition (PPCI) is a single fuel strategy that uses high levels of cooled exhaust gas recirculation (EGR) combined with high-pressure fuel injection (Jacobs, 2007). Reactivity controlled compression ignition (RCCI) is a dual fuel LTC strategy that uses a premixed charge of a low reactivity fuel such as gasoline combined with direct injection of a high reactivity fuel such as diesel during the compression stroke (Reitz and Duraisamy, 2014).

The use of LTC in CI engines is known to emit greater unburned and partially burned hydrocarbon (HC) emissions compared to CDC. Jacobs (2007) showed double the HC emissions for PPCI versus CDC at the same engine speed and load. Prikhodko et al. (2010) showed an order of magnitude increase in HC for low load RCCI compared to equivalent speed and load CDC. These emissions contain a range of organic compounds with molecular weight ranging from methane to unburned fuel molecules and heavy polycyclic aromatic (PAH) compounds (Merritt et al., 2006). In-cylinder formation mechanisms and speciation of HCs from LTC have been studied (Knafl, et al. 2006; Colban et al. 2007; Han et al. 2008). Although solid particle mass concentrations are very low for LTC, high concentrations of semi-volatile HC in LTC exhaust are known to form nanoparticles through nucleation and growth mechanisms upon primary dilution (Northrop et al. 2011a). Further, we have shown in previous work that volatile material can slip through a close-coupled aftertreatment system composed of a diesel oxidation catalyst (DOC), and diesel particulate filter (DPF) and form particles under certain conditions (Lucachick et al., 2015). Although considerable research has characterized nanoparticles from CDC, very little has been done to specifically examine semi-volatile nanoparticles from LTC operation in CI engines.

Given high gas-phase semi-volatile HC concentration, measurement of LTC nanoparticle mass and number is highly dependent on dilution conditions. Filter sampling of volatile particles is known to result in artifacts like semi-volatile gas-phase adsorption on the filter medium or captured volatile particles evaporating before gravimetric measurement (Liu et. al 2012). Sample instability renders it difficult to assess environmental and health effects or ensure regulatory

compliance of LTC particles using gravimetric-based methods. As an example, Kolodziej et al. (2007) reported up to a 46 times difference in the elemental carbon to organic carbon ratio on collected filters from a mid-load LTC condition using three independent analysis methods. Unburned fuel is thought to heavily contribute to LTC-derived primary particles, but previous work has shown unburned fuel alkanes are not solely responsible for the increase in volatile particle emissions (Northrop et al. 2011a). Other contributing species include low volatility components like methyl ester in biodiesel and polycyclic aromatic hydrocarbons (PAHs) present in diesel fuel and from combustion. The study by Merritt et al. (2006) on unregulated emissions from CDC and LTC showed orders of magnitude increases of particle forming PAH compounds for LTC modes in comparison to CDC modes. Other studies suggest that species beyond PAH and unburned fuel contribute to LTC particles. Sluder et al. (2004) deduced that in addition to unburned fuel species and PAH, additional semi-volatile species likely include carboxylic acids and long-chain aldehydes. Another source of volatile particle forming material not exclusive to LTC is unburned lubricant oil, though the particle mass contribution from oil is small compared to the contribution from fuel (Franklin, 2010).

Literature is sparse regarding particle emissions from dual-fuel RCCI operation. In a study by Dempsey et al. (2014), a two-stage high temperature dilution process resulted in large reductions in particle mass and number concentration for increasing dilution ratio and increasingly high temperature dilution for several RCCI speed and load conditions compared to CDC operation. Additionally, the same authors reported elevated HC emissions, implying the potential for semi-volatile particle growth at lower dilution temperature. In our previous work, we also found that

RCCI combustion results in high concentrations of HC compounds that can slip through conventional DOC aftertreatment and form nucleation mode particles (Prikhodko et al., 2013, Storey et al., 2015). RCCI was shown to result in higher overall particle mass concentration then PPCI at tested dilution conditions though particles from both modes primarily consist of semi-volatile organics.

To date, accurate characterization of primary nanoparticles from LTC has been largely stymied by their high semi-volatile content. Here, we present a comprehensive overview of LTC nanoparticle volatility by experimentally comparing PPCI and RCCI operating modes using evaporative tandem differential mobility analysis (V-TDMA). Volatility data is then used to elucidate the general composition of particles by comparing with single component evaporation data and a phenomenological condensation and evaporation model.

METHODS

ENGINES AND FUELS

PPCI and RCCI combustion mode experiments were conducted on separate light-duty multi-cylinder direct-injection turbocharged diesel engines. For PPCI, a 1.96 liter displacement General Motors (GM) common-rail turbo-diesel engine with a 16.5:1 compression ratio and bowl-in-piston piston geometry was used. RCCI experiments were conducted using a 1.91 liter GM common-rail turbocharged diesel engine with a 17.5:1 compression ratio and bowl-in-piston

combustion geometry. The engines were similar in design and suitable for duty in passenger vehicle applications. National Instruments hardware and software was used for engine control and data acquisition for both engines. Both engines were fueled with ultra-low sulfur diesel (ULSD) with sulfur content below 6 ppm for the directly injected fuel. In the dual-fuel RCCI engine, EEE-Lube Cert Gasoline with sulfur content of 11 ppm was used as the port-injected low-reactivity fuel.

COMBUSTION MODES AND TEST PROCEDURE

Several steady-state low to intermediate loads from 2 to 5.6 bar brake mean effective pressure (BMEP) were used in PPCI and RCCI combustion modes. For PPCI, a 1500 rpm 2 bar BMEP early injection strategy, and a 1500 rpm 4 bar BMEP late injection strategy was used. For RCCI, a 1500 rpm 2.6 bar BMEP strategy, a 1500 rpm 4 bar BMEP strategy, and a 2600 rpm 5.6 bar strategy was chosen. Table 1 provides additional information about the operating modes used in this study. Further details concerning the engines and operating modes for PPCI and RCCI can be found in Lucachick et al. (2014a) and Dempsey et al. (2014), respectively. The five chosen modes represent operating conditions sufficient for propelling a mid-size passenger vehicle at low speed for the low-load cases and highway speed for the highest load case.

Table 1

GASEOUS EMISSIONS MEASUREMENT AND ANALYSIS

Measurement of gaseous NO_X, carbon monoxide (CO), and HC emissions was conducted using Fourier Transform Infrared (FTIR) analyzer for both RCCI and PPCI combustion. For RCCI combustion, a heated flame ionization detection (FID) instrument was used for measurement of total HC on a C_1 basis. For PPCI, total HC was estimated using a weighted summation of the HC species measureable with the FTIR for representation on a C_1 basis.

PARTICLE EMISSIONS MEASUREMENT AND ANALYSIS

Soot mass emissions from the PPCI engine were measured using an AVL Microsoot photoacoustic analyzer and an AVL 415S Smoke Meter was used for the RCCI engine. Though smoke meter measurements have been shown to be to be comparable to soot mass concentration even at very low levels found in LTC modes (Northrop et al. (2011b)), such information for the photoacoustic analyzer is sparse. Future work is required to validate the accuracy of Microsoot measurements for low elemental carbon LTC particles.

Particle sizing and counting was conducted using a scanning mobility particle sizer (SMPS) comprising of a TSI 3081 electrostatic classifier and TSI 3025 condensation particle counter (CPC). To define initial conditions for the evaporation/condensation model, total particle mass emissions were estimated from SMPS results assuming particles are spherical with unity specific

gravity. To simulate primary dilution in the atmosphere under controlled temperature and flow conditions, a two-stage dilution system was used (Abdul-Khalek and Kittelson (1998)). Careful control and measurement of dilution conditions is especially important for measuring particles from LTC due to their high semi-volatile fraction. Primary dilution ratio was continually measured using a non-dispersive infrared CO_2 analyzer. Secondary dilution ratio was periodically measured before and after the experiments and found to be constant throughout the experiments. Filtered, dry, CO_2-free, and temperature controlled air was used for primary and secondary dilution. Primary dilution for all particle measurement experiments was 13.9 ± 2.6 and secondary dilution was 20.6 ± 7 resulting in a total dilution ratio of approximately 300. The secondary dilution quantity was assumed sufficient to freeze semi-volatile particles prior to SMPS measurement.

A catalytic stripper (CS) was used to remove organic material from exhaust particles. This device consisted of an oxidation catalyst core operated under controlled temperature and flow conditions (Abdul-Khalek and Kittelson, 1995). In the CS, volatile organic material is evaporated and oxidized leaving only solid particles. Remaining particles after the CS primarily consist of soot and solid ash. CS experiments allowed discernment of solid versus organic material in-situ using SMPS. An empirically derived, size-dependent loss correction factor was applied to the SMPS data to account for particle losses occurring in the CS (Lucachick et al. (2014b)).

Figure 1

Volatility tandem differential mobility analysis (V-TDMA) was used to explore particle volatility as a function of particle size (Sakurai et al. (2003a), Tao and McMurry (1989)). A diagram of the complete particle measurement apparatus is given in Figure 1. V-TDMA employs a separate differential mobility analysis (DMA) column that selects a monodisperse particle distribution from the polydisperse aerosol. In the V-TDMA study, particles sizes were selected for each engine mode that corresponded to the number distribution maximum for lowest and highest loads. Dilution temperature was controlled to 36 °C and 27 °C for the RCCI and PPCI operating modes, respectively. The monodisperse aerosol was then subjected to controlled elevated temperature conditions as it flowed through a tube submerged in an oil bath to maintain isothermal conditions. Changes in particle size due to evaporation were then measured by SMPS and analyzed as a function of evaporator residence time and temperature. Smaller selected monodisperse aerosols were measured using a TSI 3080 nano-DMA for the V-TDMA experiments.

Figure 2

Measuring evaporation rates of pure compounds provides a valuable volatility benchmark from which to compare exhaust particles. An evaporative particle generator (EPG) was used to create heavy alkane particles as a baseline comparison for LTC exhaust particles. The resulting particles were processed with the V-TDMA and the particle size reduction was measured using

SMPS. A schematic of the EPG apparatus is shown in Figure 2. Primary dilution ratios for the EPG experiments were identical to the engine experiments to ensure data comparability.

Uncertainty of the SMPS measurements was estimated as one standard deviation from three scans taken per condition. Repeatability was verified by testing using one engine condition on separate days for each RCCI and PCCI engine modes and factored into overall uncertainty reported as error bars in this paper using a root mean square approach. The numerical sequential perturbation method (Figliola (2000)) was used to propagate uncertainty through the geometric mean diameter calculation.

RESULTS AND DISCUSSION

NO_X, SOOT, CO, HC EMISSIONS

Emissions of NO_X, consisting of NO and NO_2, and soot for the PPCI and RCCI modes tested in the experimental study were comparable to our previous work with the same engines at similar engine load conditions and are significantly lower than comparable CDC engine conditions (Lucachick et al. (2014a), Prikhodko et al. (2010), and Storey et al. (2008)). Error bars represent the standard error of the mean of each dataset. Standard errors are not available for the RCCI data since only three samples were taken per condition using the AVL Smoke Meter. As shown in Figure 3a, RCCI NO_X emissions were higher than PPCI at similar engine operating conditions. Soot mass emissions were similar for PPCI and RCCI modes, however 2 bar PPCI delivered the

lowest soot emissions of all tested combustion modes and the 4 bar PPCI case had the highest soot mass concentration.

HC and CO emissions were also in agreement with prior literature and are given in Figure 3b. CO emissions were similar for all modes, and several times higher than CDC from similar loads run in prior studies. The 2 bar PPCI operating point exhibited the highest CO levels, with the highest EGR levels contributing to low combustion temperatures and the highest equivalence ratio of all the modes in the study. Gaseous HC emissions were found to be approximately three times higher for RCCI modes than for PPCI operation.

Figure 3

DILUTION SENSITIVITY OF LTC PARTICLES

Previous studies have shown that a large soot accumulation mode serves as a sink for volatile vapors, thereby suppressing formation of nucleation mode particles (Bagley et al., 1996, Khalek et al., 2000). We showed the same phenomenon in previous work (Lucachick et al. (2014a)) where a large accumulation mode in CDC exhaust suppressed semi-volatile nucleation mode particle formation over a range of dilution temperature. Low soot levels also resulted in greater overall particle sensitivity to dilution conditions due to fewer solid sites for gas to particle conversion. This effect is extremely pronounced for LTC combustion modes that emit extremely

low soot levels. Figure 4 shows that the RCCI and PPCI cases considered here exhibited high sensitivity to dilution temperature. Lower dilution temperatures can result in particle vapor precursor saturation ratios that increase by orders of magnitude, as will be discussed. Number concentration and geometric mean diameter (GMD) for all combustion modes are given in Table 2. The total particle number concentration increased by approximately one order of magnitude with decreasing dilution temperature while GMD decreased indicating a shift to nucleation mode particles.

Figure 4

Post-CS number concentration results show that semi-volatile particles contribute to the vast majority of total particle number. Figure 4 illustrates that post-CS number concentration was approximately two orders of magnitude lower than the number concentration for the cool dilution case for both combustion modes, and approximately one order of magnitude lower than for the warm dilution cases. One exception is seen in comparing warm dilution and CS number concentrations for 4 bar PPCI. The CS number concentration for the 4 bar PPCI point was approximately half that of warm dilution number concentration for the same mode. Although low, this combustion mode had the highest soot concentrations of any of the tested modes as confirmed in Figure 3. This soot existed in sufficient quantities to absorb the particle forming material and suppress the formation of large quantities of nucleation mode particles.

Table 2

V-TDMA RESULTS

Size dependent particle volatility and external mixing characteristics were explored using V-TDMA. Here, monodisperse particle distributions of different particle diameter were selected using DMA for RCCI and PPCI combustion modes. As shown in Figure 5, particles were selected at the maximum of the number distribution for the high and low load cases for each combustion mode. PPCI particles were selected using nominal DMA voltages of 80 and 340 to investigate nanoparticles with diameters of 18.9 nm and 40.2 nm, respectively. RCCI particles were selected using nominal DMA voltages of 40 and 200 to measure similarly sized nanoparticles at 13.3 nm and 30.4 nm, respectively. After DMA selection, particles not subjected to thermal conditioning were measured by SMPS at 5% smaller than predicted by classifier theory. The cause of this discrepancy is not fully understood, but the highly volatile nature of the particles may have resulted in particle shrinkage during and after traversing the classifier despite the lack of conditioning. This phenomenon was not verified using solid particles, so neither the DMA nor the particles themselves were identified as the source of the discrepancy. Other experimental errors could have included aerosol or sheath flow control errors. To account for size selection error, particles were selected and measured directly by SMPS to identify the initial particle size before thermal conditioning.

Figure 5

Figure 6a shows the effects of thermal conditioning on RCCI particles. A conditioning temperature of 105 °C produced similar reductions in particle diameter for all RCCI loads for particles selected at 13.3 nm, with an average diameter reduction of 8 nm ± 2. This represents an average reduction in particle volume of 94%. Conditioning temperature of 105 °C resulted in diameter reductions of similar magnitude, averaging 16.3 ± 2 nm for all three loads. This reduction in diameter reduces particle volume by an average of 94%. Similar to particles selected at 13.3 nm, at least 94% of the particle volume was completely volatile for 30.4 nm diameter particles.

The effects of thermal conditioning on PPCI exhaust particles are shown in Figure 6b. For particles selected at 18.9 nm, conditioning to 110 °C for 4 bar PPCI and 125 °C for 2 bar PPCI resulted in total particle volume reduction of 87% and 91%, respectively. For particles selected at 40.2 nm, conditioning to 110 °C for LLTC and 125 °C for ELTC resulted in particle volume reductions of 86% and 96%. Our previous work has shown that the solid fraction of PPCI particles is greater than RCCI (Prikhodko et al., 2013). However, for the experiments conducted, soot mass concentrations for RCCI and PPCI (Figure 3) were comparable and V-TDMA results indicate similar volatility profile for the two combustion modes. Figure 4 indicates that PPCI particles exhibit a more pronounced accumulation mode than RCCI after CS processing, providing some evidence that there were more solid carbon agglomerates for the PPCI case than for RCCI. Regardless, the fractional volume reductions for PPCI particles were similar to RCCI particles, indicating that they were mostly comprised of volatile material.

Figure 6

The catalytic stripper results (Figure 4) show that at the sizes selected for V-TDMA, there is an order of magnitude reduction in particle number as compared to results without catalytic stripper, thus the vast majority of particles at these sizes can be assumed to be volatile with no solid core. The V-TDMA results in Figure 6 show that for both RCCI and PPCI, larger particles experience greater reductions in diameter compared to smaller particles at a given conditioning temperature. If smaller particles had exactly the same composition as larger particles, they would experience greater reductions in diameter at a given conditioning temperature due to evaporation enhanced by the Kelvin effect. The opposite is true in our results, providing evidence that the smaller particles are comprised of overall lower volatility material. This phenomenon is distinctly different than the trend common to CDC particles consisting of a volatile nucleation mode and a sooty, nonvolatile accumulation mode (Sakurai et al. 2003a). Our finding of decreasing volatility with decreasing particle diameter is consistent with observations made by Shiraiwa et al. (2013) on secondary organic aerosols produced in an environmental chamber using dodecane and ammonia sulfate seed particles where higher volatility material preferentially partitioned to larger particle sizes. It is likely that the same phenomenon occurs with LTC-generated particles in the primary exhaust plume.

In Figure 6, exhaust particle diameter reduction of selected 30.4 nm and 40.2 nm particles are compared to particle diameter reduction of pure C_{28} and C_{32} particles of the same size generated with the EPG apparatus. Uncertainties for the engine condition data shown in the figure were

approximately the same magnitude as for the EPG experiments but error bars were omitted from the plot for clarity. The two selected alkanes in the EPG experiments spanned the center of a response curve for gas-chromatography analysis of engine oil in Sakurai et al. (2003b). Additionally, pure alkanes are a good surrogate for volatile exhaust particles because they are inert, nontoxic, prevalent in diesel exhaust particles, and are a primary component of petroleum diesel fuel. (Chickos and Hanshaw, 2008). Alkane particles were created in the EPG and size selected using DMA voltages of 200 and 340. At low to moderate conditioning temperature, RCCI and PPCI particles evaporated less than C_{32} particles, but more than C_{28} particles indicating that their overall volatility fell in between the two pure alkanes. For high conditioning temperatures, exhaust particles experienced less evaporation than both pure alkane types, illustrating that residual low volatility components remained in the engine-produced aerosols. Evaporation resistance at high conditioning temperature highlights the wide range of volatilities of compounds comprising LTC particles and further substantiates our finding of low volatility compounds contained within the exhaust particles.

Figure 7

Estimated saturation ratios of candidate alkanes were also calculated to explore particle growth under a variety of dilution temperatures. Total particle volume assuming spherical particles comprised of C_{28} and C_{32} alkanes were used to estimate pre-dilution particle-forming vapor concentrations in the experimental data. Saturation ratios as a function of temperature were estimated using the 2.6 bar RCCI particle volume data after primary dilution using relations

developed by Chickos & Hanshaw (2004) for alkane saturation pressure and are shown in Figure 7. The calculation used the conservative assumption that the entirety of the precursor vapors transitioned to particle phase, making the entire precursor volume concentration measurable using SMPS. Saturation ratios are two orders of magnitude greater for C_{32} than C_{28} for all temperatures, and are more than an order of magnitude larger than unity for both compounds for all temperatures investigated. This implies that volatility of oil and fuel alkanes in this volatility range is sufficiently low to promote condensation on existing particles under the observed dilution conditions.

Critical saturation ratios (S_{crit}) required to homogeneously nucleate these alkanes were also calculated using classical nucleation theory and methods found in Rusyniak et al (2001) and shown in Figure 7. Further details regarding nucleation calculations are found in the online Supplemental Information. S_{crit} values for both compounds were orders of magnitude higher than the measured saturation ratios S. This suggests that despite large saturation ratios, these compounds are unlikely to form particles through homogeneous nucleation. Therefore, it can be concluded that although these compounds will condense onto existing particles, it is very unlikely that they would homogeneously nucleate on their own. Thus, we hypothesize that other condensation nuclei formed from sulfuric acid or other ultra-low volatility material most likely act as nucleation sites of semi-volatile LTC particles.

EVAPORATION/CONDENSATION MODEL RESULTS

To validate the observation that smaller particles from LTC possess lower volatility than larger particles, a phenomenological aerosol evaporation and condensation model was used to study the gas to particle partitioning process under transient dilution conditions. This model used multicomponent evaporation/condensation theory from Vesala et al. (1997) to calculate the time-dependent evolution of particles made of three components. Details regarding the evaporation/condensation model are found in the online Supplemental Information.

As shown in the comparison to pure alkanes in Figure 6, the V-TDMA experiments indicate that the bulk of the initially evaporating LTC particle material spans a volatility range between C_{28} and C_{32} alkanes, with a portion of particles having lower volatility and thus more resistance to evaporation at high thermal conditioning temperatures. Based on these results, three volatile material surrogates were chosen for examination using the evaporation model. An alkane between the two studied experimentally using the EPG and V-TDMA (C_{30}) was chosen combined with one with higher volatility (C_{25}) and one with lower volatility (C_{35}). Using the same estimated vapor precursor concentrations used in the saturation ratio calculations from the 2.6 bar RCCI condition, the initial conditions assumed a Poisson-distributed particle distribution of initially incepted clusters with a mode diameter of 10 nm comprising a total volume equal to one third of the available vapor precursors. These clusters were given the initial condition of equal volume concentrations of C_{25}, C_{30}, and C_{35} alkanes. Particles were assumed to be homogeneously internally mixed during the evaporation/condensation process. The model simulated evaporation and condensation for 1 second, which approximates the time spent in the aging tunnel after primary dilution. Because the experimental results indicated that smaller

particles were comprised of less-volatile material than larger particles, the composition history of smaller (D_P = 13.3 nm) and larger (D_P = 30.4 nm) particles were individually tracked during the simulation.

Figure 8

The results of the analysis are shown in Figure 8. It can be seen that particle size has a significant impact on condensation and evaporation mechanisms, resulting in differences in final composition. 13.3 nm particles are comprised of only 29% C_{25} after one second's aging time, while 30.4 nm particles increase to 36% C_{25} after the same time period. Due to the Kelvin effect, initial condensation of C_{25} is inhibited for both 13.3 nm and 30.4 nm particles, but the effect is much more pronounced for the 13.3 nm particles, with initial C_{25} uptake occurring at only 60% the rate of the 30.4 nm particles. Additionally, growth due to C_{25} on the 30.4 nm particles actually exceeds growth due to C_{30} and C_{35} by 0.12 seconds into the aging process. This is because the two lower volatility species became depleted in the earlier portion of the growth process, during which C_{25} condensation was inhibited by the elevated Kelvin effect due to the small initial cluster diameter.

Figure 9

The time derivative of calculated particle diameter as contributed by C_{25}, C_{30}, and C_{35} is shown for 13.3 nm and 30.4 nm in Figure 9. For both particle sizes, condensation dominates growth

contributions from C_{30} and C_{35}, as low particle surface vapor pressure mitigates evaporation of these species, even for the smaller 13.3nm particles. This results in equivalent condensation rates for C_{30} and C_{35}. Since LTC particles would be comprised of far more than three individual components, real-world atmospheric evaporation over extended time periods would result in increasingly lower volatility for small particles. As suggested previously, this gives further evidence that the same mechanisms responsible for partitioning of volatile material to the particle phase over long time periods for secondary organic aerosols can act on primary LTC exhaust particles on a much shorter time scale.

CONCLUSIONS

Results of this work show that volatile composition of particles emitted by LTC in CI engines confers particle formation mechanics and mixing characteristics unlike known mechanisms for CDC particles. Both single-fuel PPCI and dual-fuel RCCI particle formation is highly dependent on dilution temperature, with particle number concentrations increasing by orders of magnitude for modest decreases in dilution temperature. Particles from CDC are known to be much more insensitive to dilution temperatures than LTC particles due to higher soot fraction.

In an additional contrast to CDC particles that generally exhibit a volatile nucleation mode and a sooty, nonvolatile accumulation mode, V-TDMA results show that smaller LTC particles are comprised of lower volatility material than larger LTC particles. Results also indicate that LTC particles are composed of a wide variety of volatile materials, with evaporation rates similar to

pure C_{28} alkane at low temperatures, and greater than evaporation rates for pure C_{32} at higher temperatures. A phenomenological particle evaporation and condensation model using pure alkanes above, within, and below this range as surrogate volatile material shows that the Kelvin effect has a significant impact on particle composition during the aging process. The effect causes reduced condensation of more-volatile material that may condense in early high saturation ratio conditions and relegates condensation of this more-volatile material to larger particles.

This study conclusively shows that the volatility range of LTC particles mostly falls within the volatility range of alkanes similar to components in engine lubricating oil. In examining the critical saturation ratios of these alkanes, homogeneous nucleation is not possible. Therefore, other extremely low volatility material is responsible for initiating nucleation of volatile LTC particles. The overall composition of LTC particles is still not fully known and these low volatility compounds could consist of a combination of sulfuric acid, heavy fuel species, lubricating oil components, PAH, and possibly oxygenated organic species such as dicarboxylic acids and aldehydes. Additional work should be performed to speciate LTC particles for quantification of the components responsible for their nucleation in the exhaust plume.

The primarily volatile nature of LTC particles poses additional concern for their removal using traditional engine aftertreatment solutions as prior studies have shown that LTC forming material can slip through a DOC-DPF aftertreatment system and form particles under certain conditions. The findings of this research are significant in that whereas the characteristics of CDC particles are known, LTC particles have not been extensively studied. Due to their differences in

composition and physical properties, regulatory rules and measurement methods designed for CDC particle emissions may not be appropriate for LTC particle emissions. More specifically, PM sample collection by filtration as required by some regulations will result in the collection of mass that may not represent the mass of primary aerosol emitted by the engine.

ACKNOWLEDGEMENTS

The University of Minnesota authors would like to thank the Oak Ridge National Laboratory Fuels, Engines, and Emissions Research Center for funding the accommodations of G. Lucachick, and providing a complete test cell, instrumentation, and operating expertise for the RCCI measurements conducted in this study. The authors would also like to thank Prof. David Kittelson at University of Minnesota for his technical guidance in designing and conducting the experimental study. Funding of the University of Minnesota portion of this work was provided by a research gift from General Motors. The ORNL authors gratefully acknowledge the support and guidance of Gurpreet Singh, Ken Howden, and Leo Breton in the US Department of Energy Vehicle Technologies Office.

REFERENCES

Abdul-Khalek, I. S., & Kittelson, D. B. (1995). Real time measurement of volatile and solid exhaust particles using a catalytic stripper (No. 950236). SAE Technical Paper.

Abdul-Khalek, I. S., Kittelson, D. B., Graskow, B. R., Wei, Q., & Bear, F. (1998). Diesel exhaust particle size: measurement issues and trends (No. 980525). SAE Technical Paper.

Bagley, S. T., Baumgard, K. J., Gratz, L. D., Johnson, J. H., & Leddy, D. G. (1996). Characterization of fuel and aftertreatment device effects on diesel emissions. Research report (Health Effects Institute), (76), 1-75.

Colban, W. F., Miles, P. C., & Oh, S. (2007). On the cyclic variability and sources of unburned hydrocarbon emissions in low temperature diesel combustion systems (No. 2007-01-1837). SAE Technical Paper.

Chickos, J. S., & Hanshaw, W. (2004). Vapor pressures and vaporization enthalpies of the n-alkanes from C21 to C30 at T= 298.15 K by correlation gas chromatography. Journal of Chemical & Engineering Data, 49(1):77-85.

Chickos, J. S., & Hanshaw, W. (2004). Vapor pressures and vaporization enthalpies of the n-alkanes from C31 to C38 at T= 298.15 K by correlation gas chromatography. Journal of Chemical & Engineering Data, 49(3):620-630.

Dempsey, A., Curran, S., Storey, J., Eibl, M., Pihl, J., Prikhodko, V., Wagner, R., & Parks, J. (2014). Particulate Matter Characterization of Reactivity Controlled Compression Ignition (RCCI) on a Light Duty Engine (No. 2014-01-1596). SAE Technical Paper.

Figliola, R., and Beasley, D. (2000). Theory and Design for Mechanical Measurements (3rd ed.). JohnWiley and Sons, New York.

Franklin, L. (2010). Effects of homogeneous charge compression ignition (HCCI) control strategies on particulate emissions of ethanol fuel (Doctoral dissertation, UNIVERSITY OF MINNESOTA).

Han, M., Assanis, D. N., & Bohac, S. V. (2008). Comparison of HC species from diesel combustion modes and characterization of a heat-up doc formulation. International Journal of Automotive Technology, 9(4):405-413.

Jacobs, T. J., & Assanis, D. N. (2007). The attainment of premixed compression ignition low-temperature combustion in a compression ignition direct injection engine. Proceedings of the Combustion Institute, 31(2):2913-2920.

Kittelson, D. B. (1998). Engines and nanoparticles: a review. Journal of Aerosol Science, 29(5):575-588.

Khalek, I. A., Kittelson, D. B., & Brear, F. (2000). Nanoparticle growth during dilution and cooling of diesel exhaust: Experimental investigation and theoretical assessment (No. 2000-01-0515). SAE Technical Paper.

Knafl, A., Jacobs, T. J., Bohac, S. V., & Assanis, D. N. (2006). The load limits of low temperature premixed compression ignition diesel combustion. Proc. of the 2nd International Symposium on Clean and High-Efficiency Combustion in Engines (ISCE 2006), (10-13).

Kolodziej, C., Wirojsakunchai, E., Foster, D. E., Schmidt, N., Kamimoto, T., Kawai, T., Akard, M., & Yoshimura, T. (2007). Comprehensive characterization of particulate emissions from advanced diesel combustion (No. 2007-01-1945). SAE Technical Paper.

Liu, Z., Swanson, J., Kittelson, D. B., & Pui, D. Y. H. (2012). Comparison of methods for online measurement of diesel particulate matter. Environmental Science & Technology, 46(11): 6127–33.

Lucachick, G., Avenido, A., Kittelson, D., & Northrop, W. (2014a). Exploration of Semi-Volatile Particulate Matter Emissions from Low Temperature Combustion in a Light-Duty Diesel Engine. SAE International Journal of Engines, 7(2014-01-1306), 852-859.

Lucachick, G., Avenido, A., Watts, W., Kittelson, D., & Northrop, W. (2014b). Efficacy of In-Cylinder Control of Particulate Emissions to Meet Current and Future Regulatory Standards (No. 2014-01-1597). SAE Technical Paper.

Lucachick, G. A., Kittelson, D., & Northrop, W. (2015). Effects of Aftertreatment on Semi-Volatile Particulate Matter Emissions from Low Temperature Combustion in a Light-Duty Diesel Engine. SAE International Journal of Engines, 8:791-796.

Merritt, P., Huang, Y., Khair, M., & Pan, J. (2006). Unregulated exhaust emissions from alternate diesel combustion modes (No. 2006-01-3307). SAE Technical Paper.

Musculus, M. P. B., Miles, P. C., & Pickett, L. M. (2013). Conceptual models for partially premixed low-temperature diesel combustion. Progress in Energy and Combustion Science, 39:246–283.

Northrop, W. F., Madathil, P. V., Bohac, S. V., & Assanis, D. N. (2011a). Condensational growth of particulate matter from partially premixed low temperature combustion of biodiesel in a compression ignition engine. Aerosol Science and Technology, 45(1):26-36.

Northrop, W. F., Bohac, S. V., Chin, J. Y., & Assanis, D. N. (2011b). Comparison of filter smoke number and elemental carbon mass from partially premixed low temperature combustion in a direct-injection diesel engine. Journal of Engineering for Gas Turbines and Power, 133(10):102804.

Prikhodko, V. Y., Curran, S. J., Parks, J. E., & Wagner, R. M. (2013). Effectiveness of Diesel Oxidation Catalyst in Reducing HC and CO Emissions from Reactivity Controlled Compression Ignition. SAE International Journal of Fuels and Lubricants, 6(2):329–335.

Prikhodko, V. Y., Curran, S. J., Barone, T. L., Lewis, S. A., Storey, J. M., Cho, K., Wagner, R. M.,& Parks, J. E. (2010). Emission characteristics of a diesel engine operating with in-cylinder gasoline and diesel fuel blending (No. 2010-01-2266). SAE Technical Paper.

Reitz, R. D., & Duraisamy, G. (2014). Review of high efficiency and clean reactivity controlled compression ignition (RCCI) combustion in internal combustion engines. Progress in Energy and Combustion Science, 46:12–71.

Rusyniak, M., Abdelsayed, V., Campbell, J., & El-Shall, M. S. (2001). Vapor phase homogeneous nucleation of higher alkanes: dodecane, hexadecane, and octadecane. 1. Critical supersaturation and nucleation rate measurements. The Journal of Physical Chemistry B, 105(47):11866-11872.

Sakurai, H., Park, K., McMurry, P. H., Zarling, D. D., Kittelson, D. B., & Ziemann, P. J. (2003a). Size-dependent mixing characteristics of volatile and nonvolatile components in diesel exhaust aerosols. Environmental Science & Technology, 37(24):5487-5495.

Sakurai, H., Tobias, H. J., Park, K., Zarling, D., Docherty, K. S., Kittelson, D. B., McMurry, P., & Ziemann, P. J. (2003b). On-line measurements of diesel nanoparticle composition and volatility. Atmospheric Environment, 37(9):1199-1210.

Shiraiwa, M., Yee, L. D., Schilling, K. A., Loza, C. L., Craven, J. S., Zuend, A., ... & Seinfeld, J. H. (2013). Size distribution dynamics reveal particle-phase chemistry in organic aerosol formation. Proceedings of the National Academy of Sciences, 110(29):11746-11750.

Sluder, C. S., Wagner, R. M., Lewis, S. A., & Storey, J. M. (2004). Exhaust chemistry of low-NOx, low-PM diesel combustion (No. 2004-01-0114). SAE Technical Paper.

Storey, J., Curran, S., Dempsey, A., Lewis, S., Walker, N. R., Reitz, R., & Wright, C. (2015). The Contribution of Lubricant to the Formation of Particulate Matter with Reactivity Controlled Compression Ignition in Light-Duty Diesel Engines. Emission Control Science and Technology, 1(64):64–79.

Storey, J. M., Lewis, S. A., Parks, J. E., Szybist, J. P., Barone, T. L., & Prikhodko, V. Y. (2008). Mobile source air toxics (MSATs) from high efficiency clean combustion: catalytic exhaust treatment effects (No. 2008-01-2431). SAE Technical Paper.

Tao, Y., & McMurry, P. H. (1989). Vapor pressures and surface free energies of C14-C18 monocarboxylic acids and C5 and C6 dicarboxylic acids. Environmental Science & Technology, 23(12), 1519-1523.

Vesala, T., Kulmala, M., Rudolf, R., Vrtala, A., & Wagner, P. E. (1997). Models for condensational growth and evaporation of binary aerosol particles. Journal of Aerosol Science, 28(4), 565-598.

Table 1. Engine operating conditions used in the experimental study.

	PPCI 2 bar	PPCI 4 bar	RCCI 2.6 bar	RCCI 4 bar	RCCI 5.6 bar
Speed (rpm)	1500	1500	1500	1500	1500
T_{intake} (°C)	64	60	35	50	35
P_{intake} (kPa)	103	110	95	101	132
Air:Fuel mass ratio	23:1	18:1	45:1	31:1	37:1
EGR (%)	64	60	33	0	0
Inj. timing (°BTDC)	20	3	51	55	62
$P_{injection}$ (bar)	800	1200	500	500	500
Gasoline Energy (%)	NA	NA	59.1	82.6	87.1

Table 2. Total particle number (TPN) concentration for warm dilution (56°C PPCI, 47°C RCCI), cool dilution (29°C PPCI, 25°C RCCI), and CS. Geometric mean diameter (GMD) for cool and warm dilution.

	TPN (10^7 #/cm^3)			GMD (nm)	
Condition	Cool	Warm	CS	Cool	Warm
PPCI 2 bar	160	10	1.6	16.0	37.4
+/-	*3.3*	*1.2*	*0.23*	*0.55*	*0.23*
PPCI 4 bar	130	5.9	4.4	24.4	43.2
+/-	*8.4*	*0.40*	*0.27*	*0.75*	*0.94*
RCCI 2.6 bar	64	8.2	0.54	15.4	26.1
+/-	*3.7*	*2.0*	*0.04*	*0.02*	*0.31*
RCCI 4 bar	7.2	2.2	0.11	17.7	22.1
+/-	*0.62*	*0.11*	*0.01*	*0.15*	*0.76*
RCCI 5.6 bar	22	3.2	0.12	16.7	19.4
+/-	*1.3*	*0.73*	*0.01*	*0.03*	*0.25*

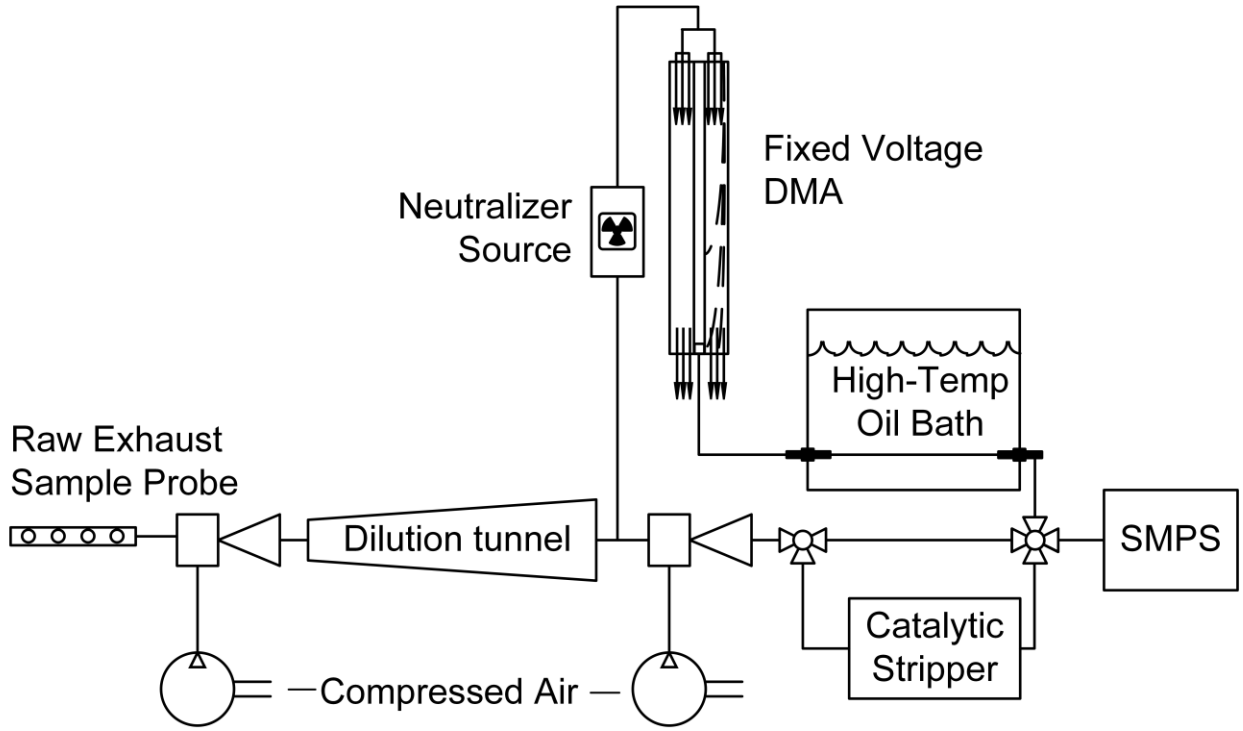

Figure 1. Particle sampling system used in the experimental study including dilution system, V-TDMA and SMPS with catalytic stripper.

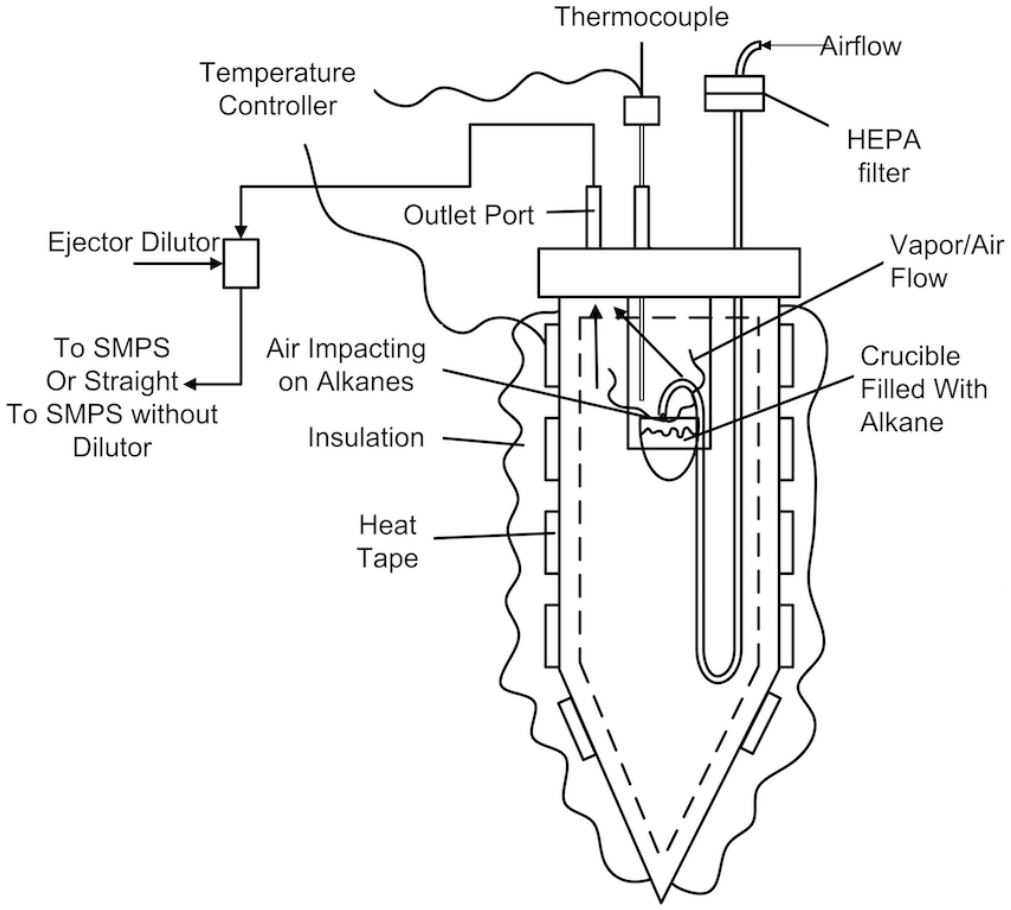

Figure 2. Schematic illustration of evaporative particle generator (EVP) used in single component V-TDMA experiments.

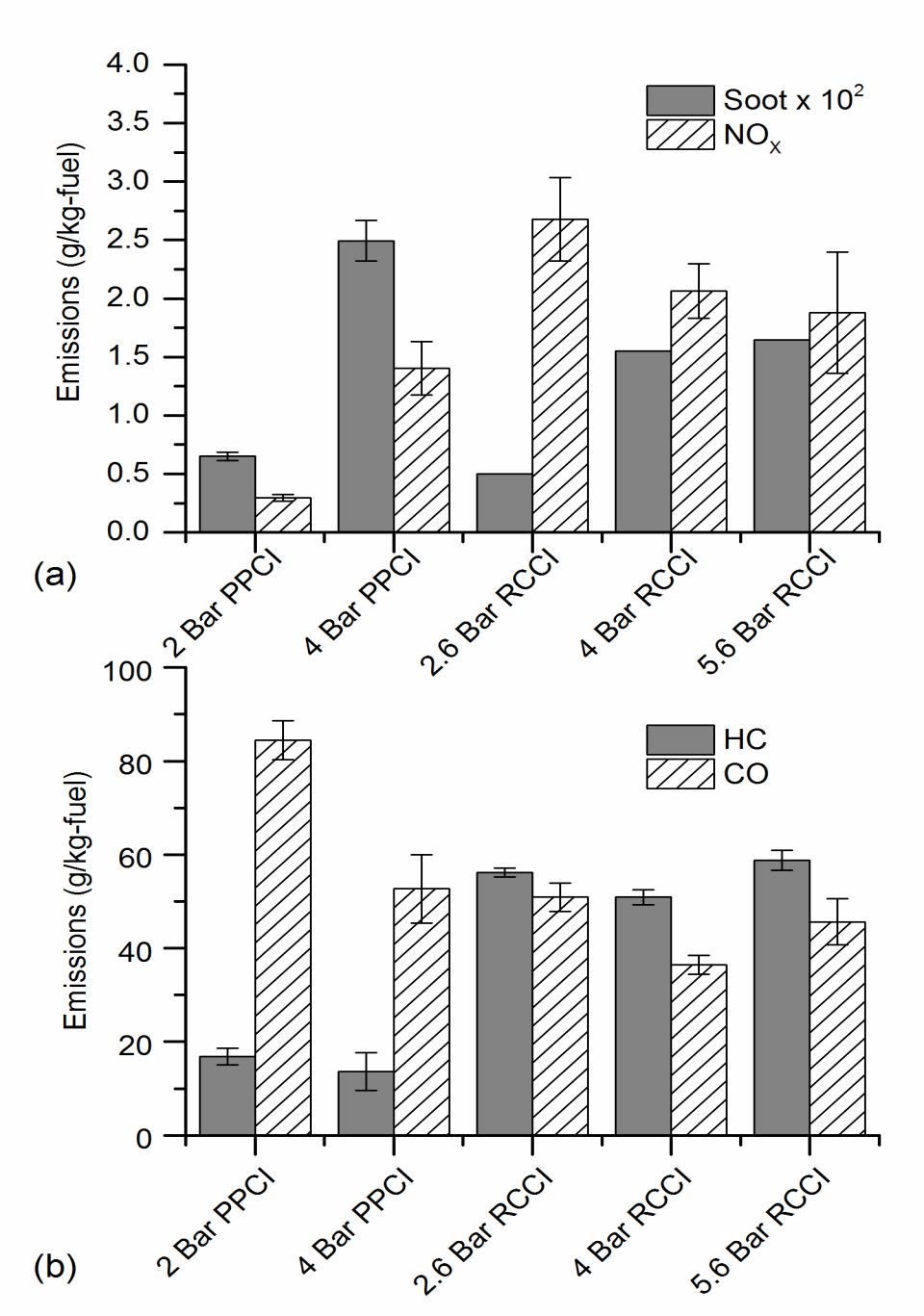

Figure 3: Emissions index in g pollutant per kg fuel for experimental engine operating conditions: (a) NOx and soot, (b) HC and CO .

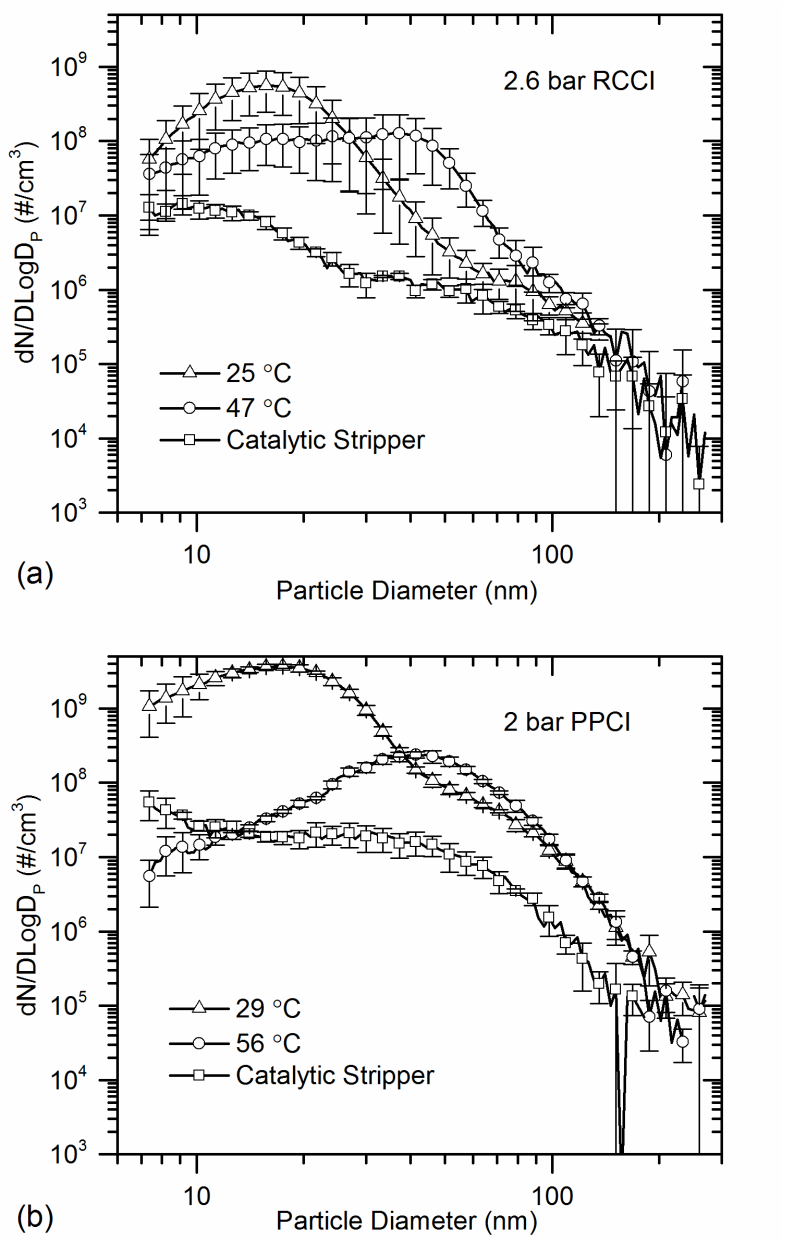

Figure 4. Total particle number distribution for two dilution temperatures and for solid particles resulting from catalytic stripper processing at engine operating conditions: (a) 2.6 bar RCCI condition, (b) 2 bar PPCI condition.

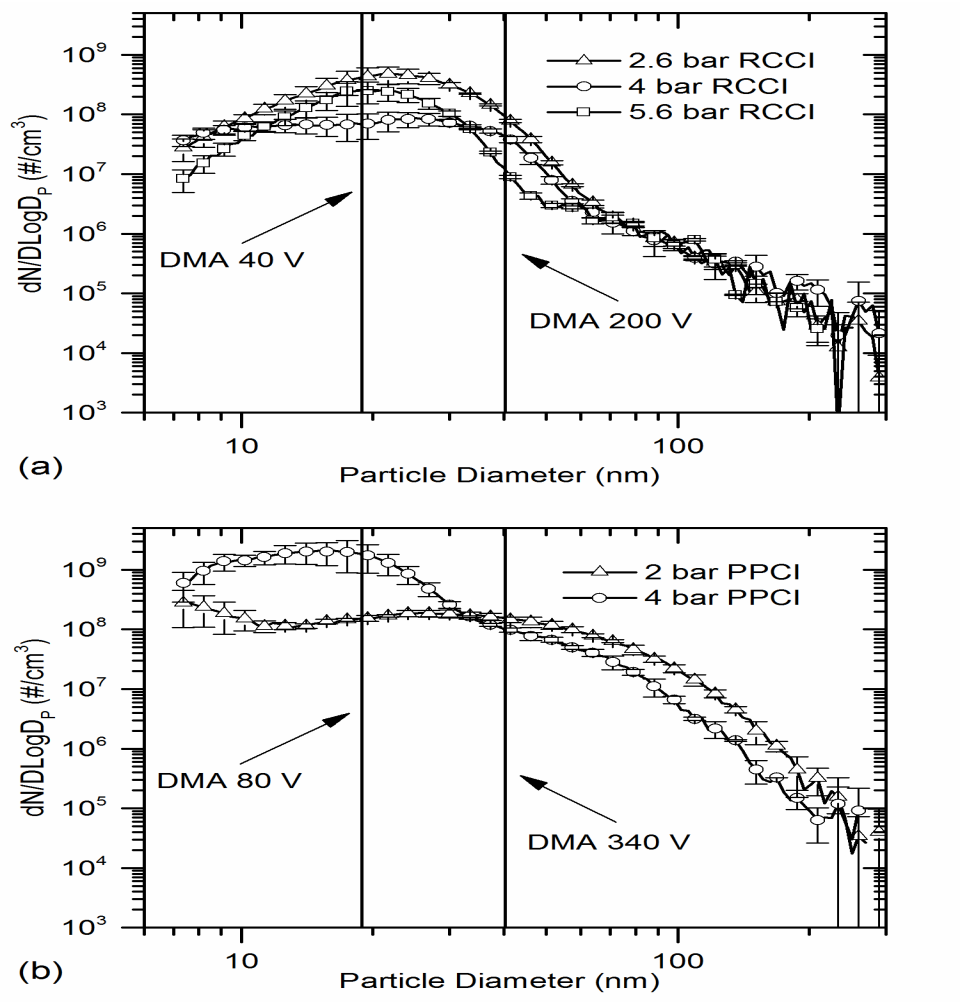

Figure 5: Particle number distributions at selected engine operating conditions showing selected DMA cut size voltages used in V-TDMA analyses: (a) RCCI with 36 °C dilution temperature, (b) PPCI particle distributions with 27 °C dilution temperature.

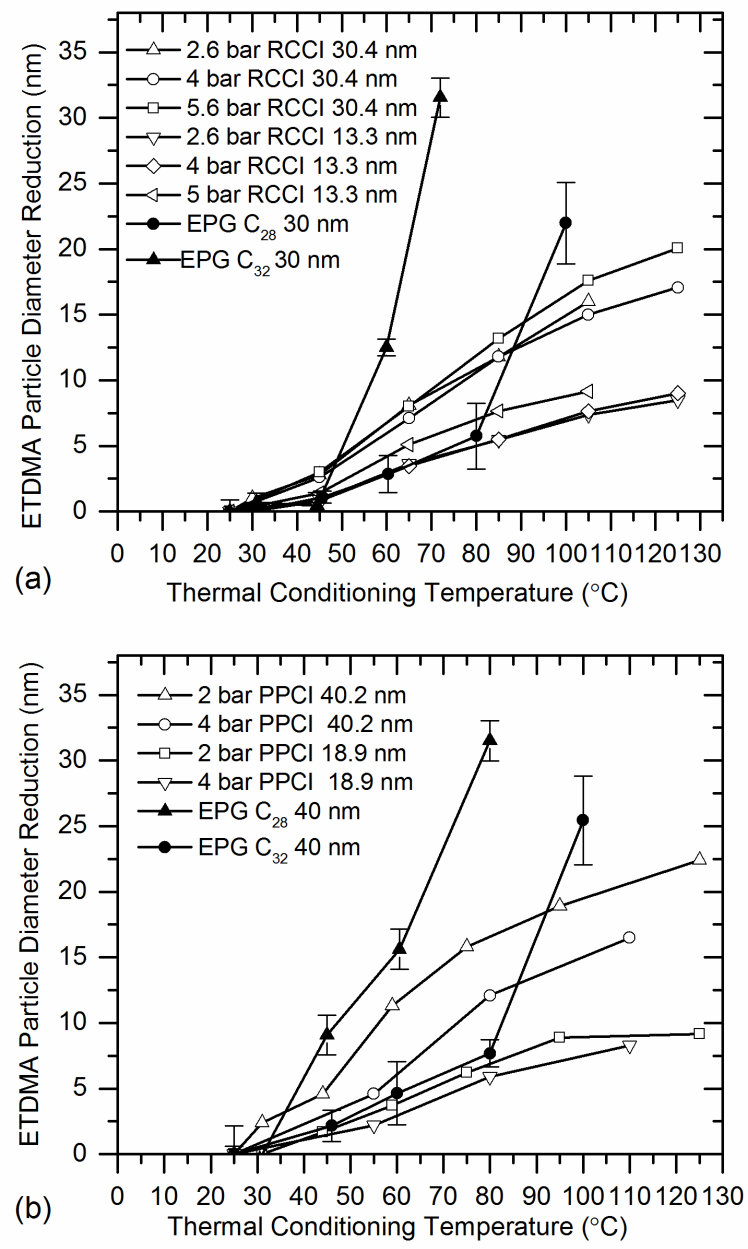

Figure 6: Reduction of particle diameter as a function of V-TDMA thermal conditioning temperature for engine-produced particles compared to pure C_{32} and C_{28} alkanes of similar particle diameter: (a) RCCI 13.3 and 30.4 nm particles (b) PPCI 18.9 nm and 40.2 nm particles.

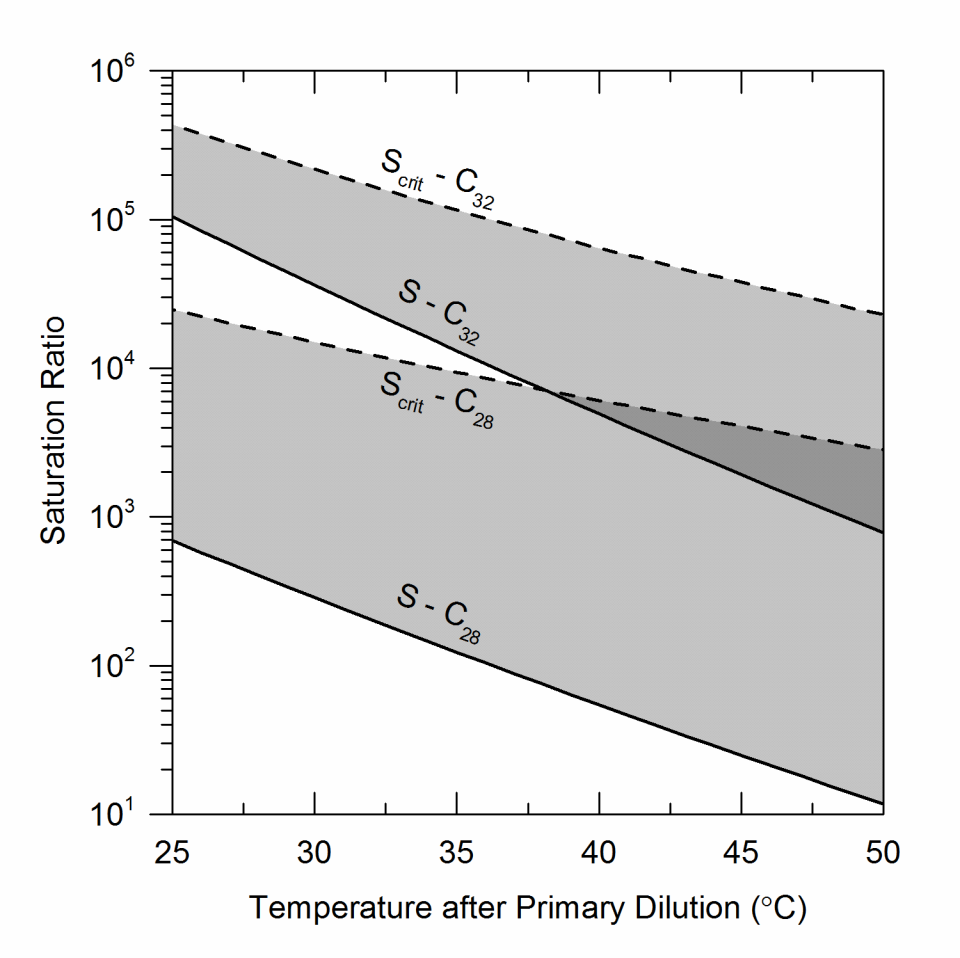

Figure 7. Calculated saturation ratio vs. dilution temperature estimated assuming total particle volume consists of solely C_{28} and C_{32} alkanes with total component mass concentrations from 2.6 bar RCCI condition used as an example.

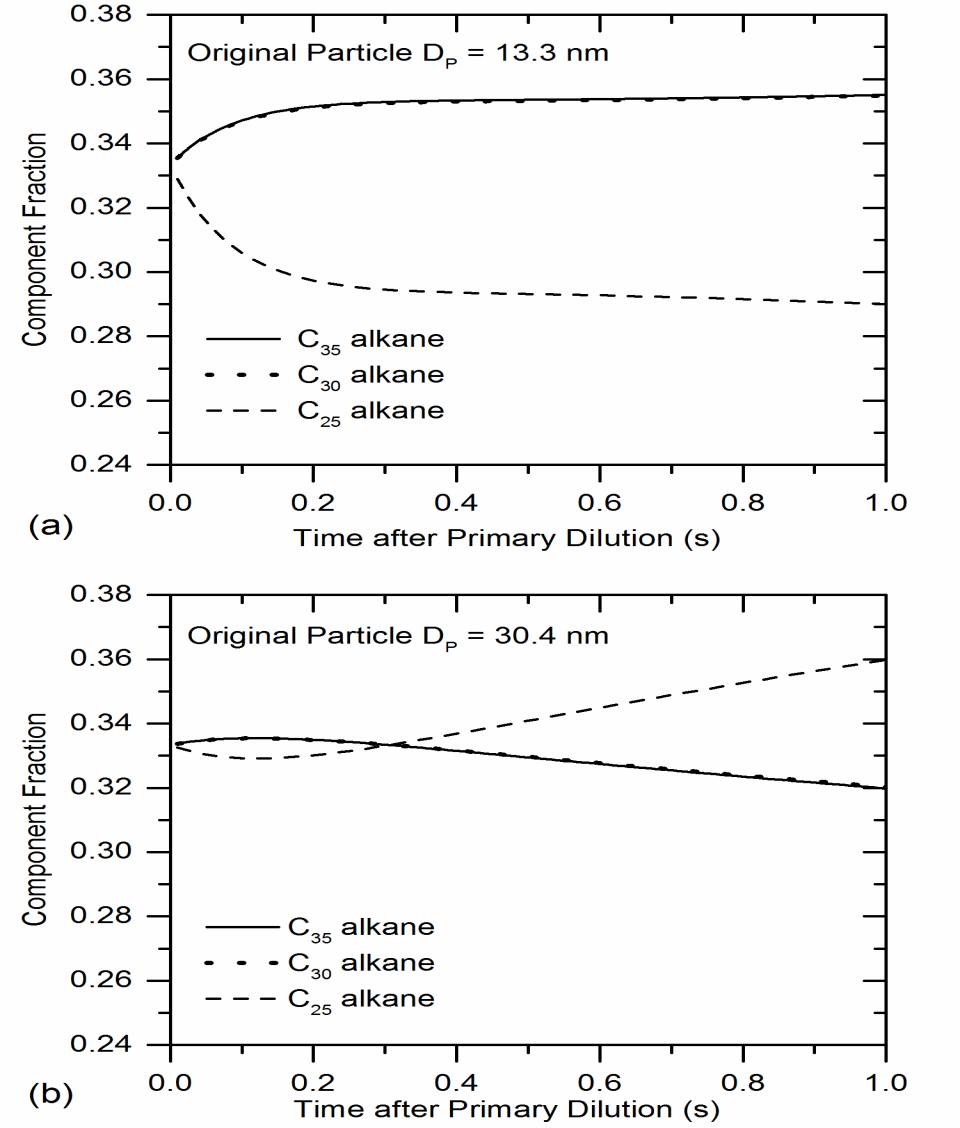

Figure 8. Simulated mass fraction history of three-component alkane particles for 2.6 bar RCCI engine condition: (a) 13.3 nm particles from 2.6 bar RCCI during primary dilution process. (b) 40.4 nm particles from 2.6 bar RCCI during primary dilution process.

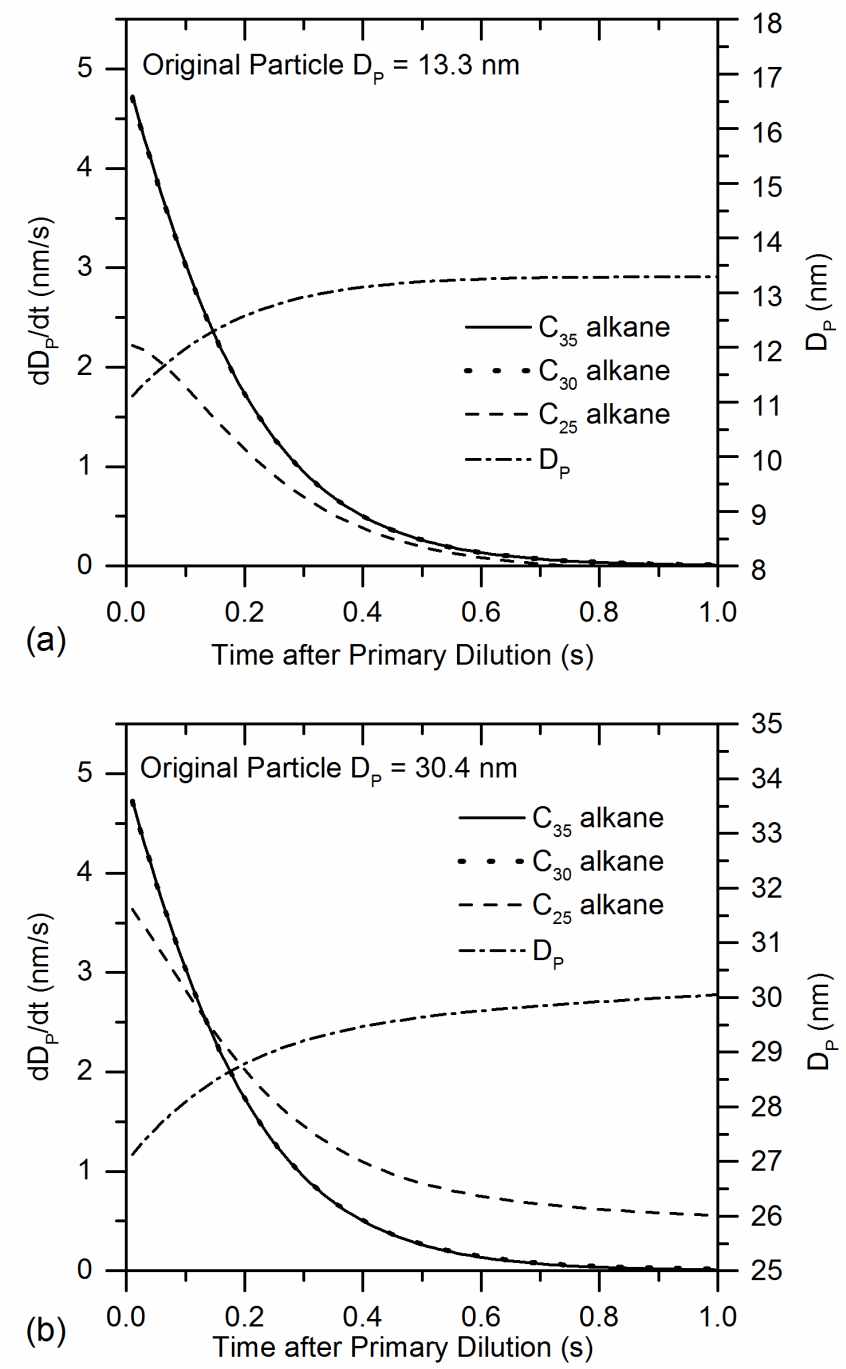

Figure 9. (a) Simulated particle growth and dD/dt contributions by component for three-component 13.3 nm particles from 2.6 bar RCCI. (b) Simulated particle growth and dD/dt contributions by component for three-component 30.4 nm particles from 2.6 bar RCCI.